Mechanism on Redistribution Synthesis of Dichlorodimethylsilane by $AlCl_3$/ZSM-5(3T)@γ-Al_2O_3 Core-shell Catalyst

Yongbing Cheng[a], Yan Wang[a], Suying Li[a], Mengsha Shen [a], Hongkun Huang[a], Mengyin Liao[a], Jiaxi Peng[a], Shunmin Ding[b], Xi Chen[a], Wenyuan Xu[a,*], Shaoming Yang[a,*]

[a] *School of Materials Science and Engineering, East China Jiao tong University, Nanchang 330013, PR China*

[b] *Key Laboratory of Jiangxi Province for Environment and Energy Catalysis, College of Chemistry, Nanchang University, Nanchang, 330031, PR China*

Corresponding authors [*] Wenyuan Xu and Shaoming Yang, School of Materials Science and Engineering, East China Jiao tong University, China, Nanchang 330013, PR China.

E-mail: xwyktz@163.com (Wenyuan Xu); yangsm@ecjtu.edu.cn (Shaoming Yang)

A B S T R A C T

The redistribution method plays an important role in addressing the issue of organosilicon by-product in the direct synthesis of dichlorodimethylsilane, and the redistribution mechanism is still a topic of debate. The redistribution by ZSM-5(3T)@γ-Al_2O_3 core-shell catalyst and post-modified $AlCl_3$/ZSM-5(3T)@γ-Al_2O_3 catalyst was technically performed using the Density Functional Theory (DFT) at the level of B3LYP/6-311++G(3df,2pd). The result shows that No.1 active site of ZSM-5(3T)@γ-Al_2O_3 core-shell structure has a significant effect on the activity of the catalyst. Indicating that the active center involved in the reaction is H provided by Al-O-H bond, which is an obvious catalytic active center of Bronsted acid. Furthermore, post-modified $AlCl_3$/ZSM-5(3T)@γ-Al_2O_3 catalyst is in more favor of redistribution reaction comparing with ZSM-5(3T)@γ-Al_2O_3 core-shell catalyst. It ascribes to the robust Lewis site of aluminum chloride favorable modification.

Keywords: Core-shell catalyst; Density Functional Theory (DFT); Dichlorodimethylsilane; Redistribution; ZSM-5(3T)

1. Introduction

Owing to the specific performance such as high and low temperature resistance, electrical insulation antioxidant stability and physiological inertia, organosilicon has a broad application prospect in fields of aerospace, electrical and electronics, architecture, medicine and chemical industry.[1-4] Besides, due to the unique structure and dual functional properties based on the combination of organic and inorganic groups, organosilicon, such as dichlorodimethylsilane ($(CH_3)_2SiCl_2$, M2), is becoming increasingly important in a wide range of scientific research and industrial processes.[5-7] However, in the synthesis of M2, chlorosilane by-products such as chlorotrimethylsilane ($(CH_3)_3SiCl$, M3) and trichloromethylsilane (CH_3SiCl_3, M1) are inevitably obtained. This problem should be resolved urgently for the sake of sustainable development and physical and mental health.[3] Traditionally, M2 can be obtained by various synthesis strategies, which can be roughly classified into four categories: direct synthesis method[3, 6, 8, 9], Grignard reagent method[10], condensation method[7] and redistribution method[11, 12]. The first three methods can produce by-products M1 and M3 in the preparation process, while the redistribution method plays an important role in transforming organosilicon by-products and resynthesizing the important silane M2, which is a waste to treasure reaction. Therefore, many studies in the past have been devoted to elucidating the mechanism of M2 disproportionation synthesis.[9, 13] The first report on the redistribution synthesis of M2 was documented by Paul D et al.[14] They used $AlCl_3$ as a catalyst. This work offered a theoretical research strategy on the thermodynamic and kinetic scales. This has stimulated interest in the search for redistributed reaction $AlCl_3$ loaded catalysts such as $AlCl_3/M_x(CO)_y$, $AlCl_3$/γ-Al_2O_3, $AlCl_3$/ZSM-5 and et al.[15-18] According to Zhenxu Chu and co-workers, Lewis acids are formed by introducing metal ions into ZSM-5 to form Si-Al bonds, and our disproportionation reaction is catalyzed by Lewis acids.[19] Our research group adopted Density Functional Theory (DFT) to conduct systematic theoretical and experimental research on the disproportionation of M1 and M3 by $AlCl_3$/ZSM-5(3T, 4T, 5T,

7T, 8T, 24T) and $AlCl_3/\gamma$-Al_2O_3 to synthesize M2, and the results showed that both $AlCl_3$/ZSM-5(3T) and $AlCl_3/\gamma$-Al_2O_3 had good catalytic effect. In particular, it was found that $AlCl_3$/ZSM-5 (3T-5T , 8T) catalysts with small clusters were more conducive to the synthesis of M2, while $AlCl_3$/ZSM-5 (7T, 24T) catalysts with rings had little catalytic activity. [20-24] Also, it is widely reported in other works that the tailored 3T cluster ZSM-5 plays a crucial role in theoretical research because of its enhanced catalytic activity.[25, 26]

At the same time, more and more literatures showed that the overall performance of core-shell materials could be significantly improved by integrating different cluster structures in the core and shell.[27-31] Therefore, if we can use the alumina support with better catalytic effect, and use the small clusters on the surface of ZSM-5 to prepare the catalyst of core-shell material, in order to achieve strong combination, and finally achieve the purpose of enhancing the catalytic effect. The idea makes us exciting.

In this paper, the core-shell catalyst with ZSM-5(3T) framework as the core and γ-Al_2O_3 as the shell was discussed. The reaction mechanism of disproportionation of M1 and M3 to prepare M2 before and after loading aluminum chloride was studied. Density functional theory (DFT)[32-34] was used to study the active site structure of core-shell catalyst, the main and side reaction channels of disproportionation reaction, the vibration modes of transition states, the energy change of reaction process, bond order, the Electronic Localization Function (ELF) and the Localized Orbit Locator (LOL) analysis were also discussed.

2 Computational details

The geometric structure of all reactants, transition states, intermediates, products and the structure of ZSM-5(3T)@γ-Al_2O_3 core-shell catalytic system and post-modified $AlCl_3$/ZSM-5(3T)@γ-Al_2O_3 catalytic system were optimized by Density Functional Theory (DFT) at the level of B3LYP/6-311++G(3df,2pd).[35] Furthermore, each transition state structure was found and calculated by TS method. All geometries were repeatedly adjusted by vibration analysis and optimized to ensure that there was only one virtual frequency for each transition state and no virtual frequency for all reactants, intermediates and products, so that the reliable and accurate information of each transition state structure was obtained.[36] Considering the calculation of the Intrinsic Reaction Coordinates (IRC),[37] all the transition state structures had a tendency towards their respective reactants and products in the forward directions, as well as in the reverse directions. Simultaneously, the correction of Zero Point Energy (ZPE) was performed to apply to the computation of each geometric optimized structure.[38] All quantum chemistry calculations were performed using the Gaussian 09 software package.

3 Results and discussion

3.1 The structure of ZSM-5(3T)@γ-Al_2O_3 and $AlCl_3$/ZSM-5(3T)@γ-Al_2O_3

The core-shell structure of the catalyst and its source and mode of combination are shown in Fig. 1 as follows: (a) The structure of γ-Al_2O_3 and its elementary unit, (b) The structure of ZSM-5 and truncated ZSM-5(3T) (c) The structure of ZSM-5(3T)@γ-Al_2O_3 and (d) Amplification structure and parameters of key active sites of $AlCl_3$/ZSM-5(3T)@γ-Al_2O_3. The geometry optimization of ZSM-5(3T)@γ-Al_2O_3 core-shell catalyst was shown in Fig. 1(c), which catalytic model consisted of γ-Al_2O_3 and 3T cluster ZSM-5 structures. In addition, ZSM-5(3T)@γ-Al_2O_3 core-shell catalyst has four Bronsted acid active sites, as shown in Fig. 1(c)(1~4). The stable core-shell structure of $AlCl_3$/ZSM-5(3T)@γ-Al_2O_3 obtained by loading $AlCl_3$ was shown in Fig. 1(d), which has two equivalent Lewis acid active sites of Al-Cl bond. Especially, the tailored 3T cluster ZSM-5 structure and the location of post-modification is very similar to that of Zhenxu Chu.[19] Also, it can be seen that the catalytic model with multiple four rings (Al-O-Al-O) is very similar to that proposed by Passana Hirunsit.[39] As can be seen from Fig. 1, the length of the Al-O

bond calculated in this paper is 0.1785-0.1980 nm, which matched with the result in the work (0.17-0.19 nm) of Sun et al.[40] In addition, the calculated Si-O bond length is 0.1670 nm and 0.1750 nm, and the experimental data is about 0.1650 nm, which deviation between the two is very small and acceptable.[41] It clearly indicates that the structure of ZSM-5(3T)@γ-Al_2O_3 core-shell catalyst is reliable. In addition, the vibration frequencies of O^1-H^1 bond, O^2-H^2 bond, O^3-H^3 bond and O^4-H^4 bond obtained through structural optimization are not significantly different, being 3677, 3684, 3688 and 3691 cm^{-1}, respectively. There is little difference between theoretical and experimental results, in which Trombetta and co-workers[42] indicated that the O-H bond

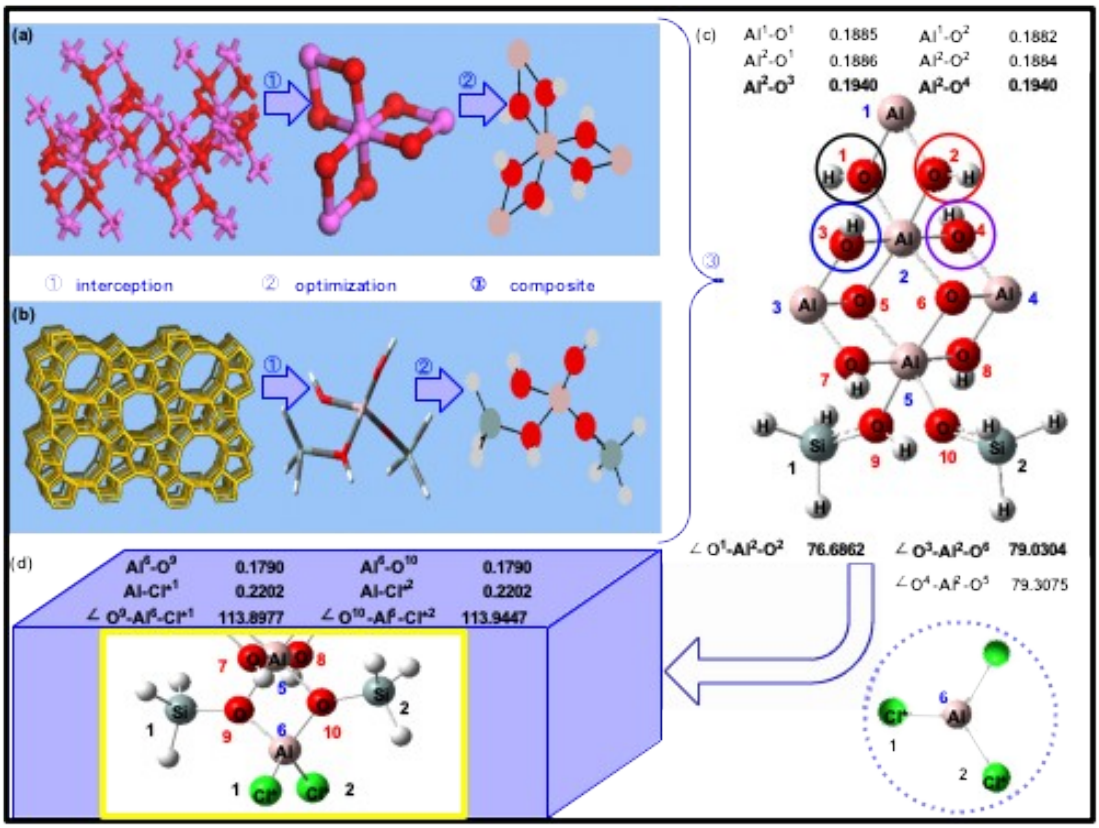

vibrated at a frequency of 3618 cm^{-1}. The deficit between our results and the reported one is below 2%. In conclusion, the structures of ZSM-5(3T)@γ-Al_2O_3 and $AlCl_3$/ZSM-5(3T)@γ-Al_2O_3 core-shell catalysts shown in Fig. 1 are credible for the following mechanic calculations.**Fig. 1**. The combined models and key atomic numbers of catalysts: (a) The structure of γ-Al_2O_3 and its elementary unit; (b) The structure of ZSM-5 and truncated ZSM-5(3T) ; (c) The structure of ZSM-5(3T)@γ-Al_2O_3 and their key parameters (bond length: nm, bond angel: °). (d) Amplification structure of $AlCl_3$/ZSM-5(3T)@γ-Al_2O_3 and their key parameters (bond length: nm, bond angel: °). ① represents the interception unit structures of γ-Al_2O_3 and 3T cluster ZSM-5, ② represents the optimization structures of γ-Al_2O_3 and 3T cluster ZSM-5, ③ represents that the catalytic model of ZSM-5(3T)@γ-Al_2O_3 is composed of as-prepared γ-Al_2O_3 and 3T cluster ZSM-5(3T) structures.

3.2 ZSM-5(3T)@γ-Al_2O_3 core-shell catalyst

Taking No.1 active site of ZSM-5(3T)@γ-Al_2O_3 core-shell catalyst as an example, the reaction mechanism on the redistribution synthesis of M2 and key atomic numbers were shown in Fig. 2. The reaction mechanism of the other three active sites is similar to that of No. 1 active site. It is clear from Fig. 2 that these reactions occur through two channels, i.e. channel 1 and Channel 2. Rx (x=1~6) represents the reactant, Px (x=1~6) represents the product and TSx (x=1~6) represents the transition state.

In the main reaction (channel 1), the catalyst firstly reacts with $(CH_3)_3SiCl$, and the O^1-H^1 bond of Al-O-H on the catalyst breaks and attacks the Si^1-C^1 bond in the silane, and then the product P1 (composed of intermediate I1 and methane) is generated through transition state TS1; intermediate I1 reacts with CH_3SiCl_3 and generates P2 (composed of main product $(CH_3)_2SiCl_2$ and intermediate I2) through TS2; I2 is easy to capture free CH_4 in a large number of catalyst beds, then P3 is formed via TS3, which makes the catalyst be reduced and the main product $(CH_3)_2SiCl_2$ is produced. In the side reaction (channel 2), the catalyst first reacts with CH_3SiCl_3, and then passes through TS4 to produce P4 (composed of intermediate I4 and methane); I4 reacts with $(CH_3)_3SiCl$, and then generates P5 (composed of intermediate I5 and by-product $SiCl_4$) through TS5; finally, I5 reacts with CH_4 and generates P6 (by-product $Si(CH_3)_4$ and the catalyst reduced) through TS6. The above reaction mechanism coincided with the experimental conclusion of Jessy Lemieux et al. which showed that the cleavage energy of Si-C bond was low and easy to fracture. It can also be seen from the figure that the active center involved in the reaction is H provided by Al-O-H bond, which is an obvious catalytic active center of Bronsted acid.[43-46]

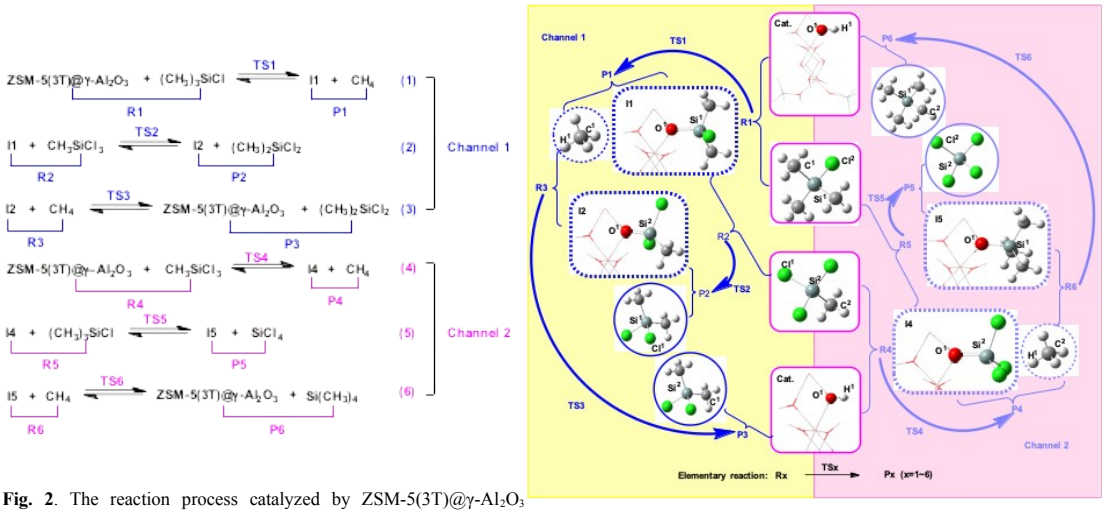

Fig. 2. The reaction process catalyzed by ZSM-5(3T)@γ-Al_2O_3 catalyst (No. 1 active site) and key atomic numbers. Rx, TSx, Ix and Px (x=1~6) represents the reactant, the transition state, the intermediate and the product, respectively. Cat. represents ZSM-5(3T)@γ-Al_2O_3 catalyst.

In Fig. 2, the changes of bond length between key atoms constitute each transition state in the reaction process. In order to verify the structural accuracy of the transition state TSx (x=1~6), the virtual vibration mode diagrams of the transition states were obtained by using vibration analysis and calculation, as shown in Fig. 3 and Fig. S1. In addition, shown in Fig. 4, IRC method was used to track the Forward and Reverse directions of transition states and the reliability of transition states was determined. Wherein negative, positive and zero represent reactants, products and transition states, respectively. Combined with Fig. 2, Fig. 3, Fig. S1 and Fig. 4, in channel 1, the atomic spacing of O^1-H^1 changes from 0.0982 nm to 0.3248 nm, and the atomic spacing of Si^1-C^1 changes from 0.1940 nm to 0.4474 nm, indicating that O^1-H^1 and Si^1-C^1 bonds are gradually separated and finally

broken. At the same time, the spacing between H^1 and C^1 changes from 0.2816 nm to 0.1093 nm, and the spacing between O^1 and Si^1 changes from 0.4197 nm to 0.1691 nm. Finally, H^1-C^1 and O^1-Si^1 bonds are formed. At this time, the transition state TS1 moves towards its corresponding product P1. Then atoms in Si^2-Cl^1 and Si^1-O^1 bonds gradually move away and finally bonds break, Si^2, O^1 and Si^1, Cl^1 move close to each other and finally form bonds. Compared with the initial atomic distance of Cl^1-Si^1 (0.4639 nm) and Si^2-O^1 (0.4829 nm) of the reactant (R2), the distance significantly decreases to 0.2182 nm and 0.1667 nm in the product P2, respectively. At this time, the transition state TS2 moves towards its product P2. Then atoms in H^1-C^1 and O^1-Si^2 bonds gradually move away and finally bonds break, while O^1, H^1 and C^1, Si^2 gradually move closely and finally bond together. The calculated atomic distances of O^1-H^1, Si^2-C^1, C^1-H^1 and O^1-Si^2 in R3 are 0.3673, 0.5054, 0.1093, 0.1668 nm, and those in P3 change to 0.0985, 0.1886, 0.4254 and 0.4467 nm, respectively. At this time, the transition state TS3 moves towards its product P3. Observing another vibrational direction of the key atoms in TS1, C^1 atom gradually approach and bond with Si^1 atom. O^1 atom and H^1 atom move closely to each other and bond finally to form its corresponding reactant R1. Other transition states can be analyzed in a similar way. The transition states in channel 2 can also move to their respective reactants and products through the corresponding atomic vibration. The longitudinal or radial stretching vibration between the key atoms is equivalent, which proves that the calculated transition state structure is correct. It can also be seen from Fig. 3, Fig. S1, Fig. S2, Fig. S3 and Fig. S4

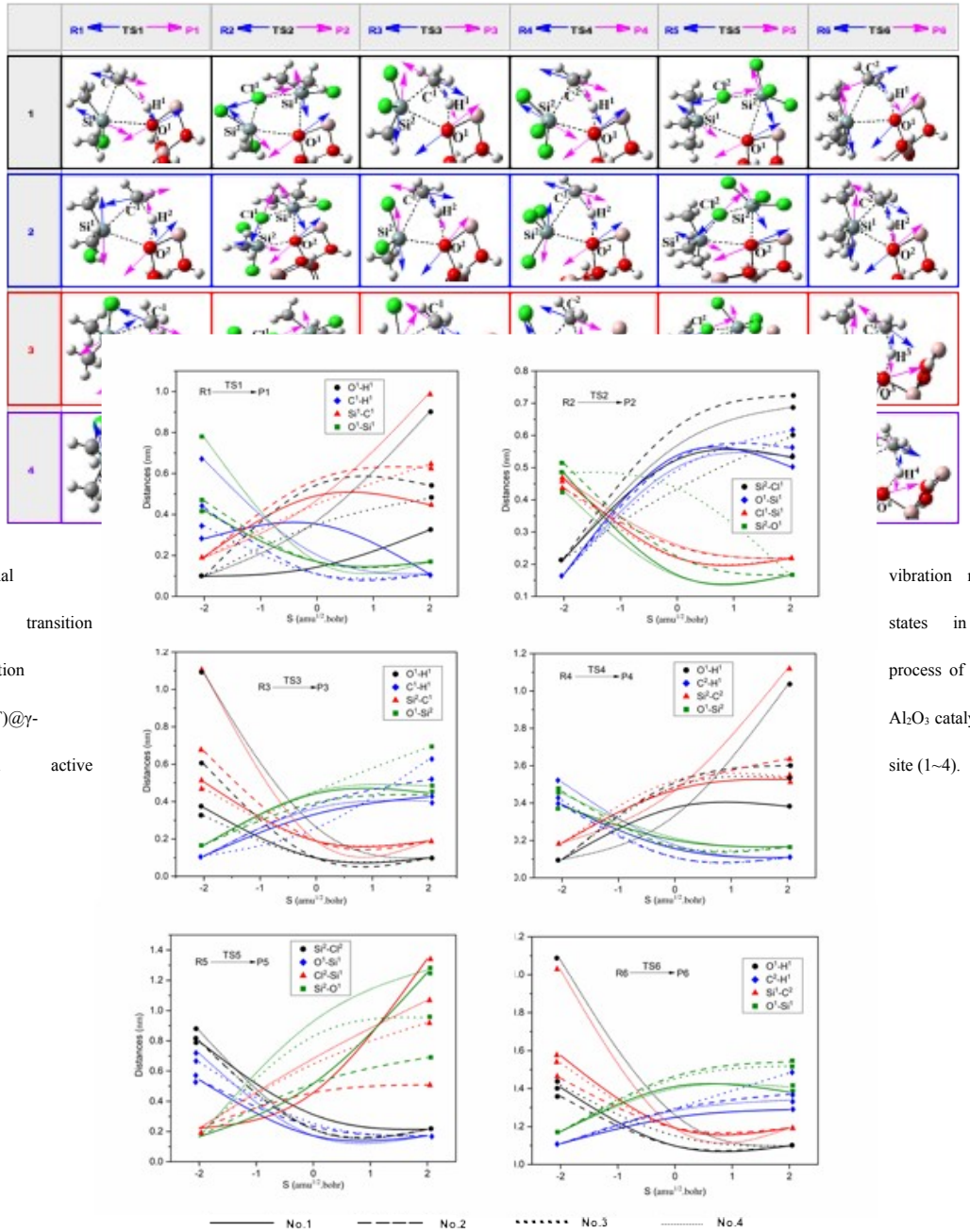

Fig. 3. The virtual vibration modes of transition states in the reaction process of ZSM-5(3T)@γ-Al_2O_3 catalyst on each active site (1~4).

Fig. 4. The spacing trends of key atoms along IRC in the catalytic system of the ZSM-5(3T)@γ-Al_2O_3 catalyst on each active site (1~4).

that the catalytic active center is the H of Bronsted acid center. The H firstly participates in the disproportionation reaction process to generate corresponding intermediates and products, and finally returns to the catalyst through the reaction channels 1 and 2, which not only realizes the recovery of the catalyst, but also realizes the generation of main products and by-products. The vibration analysis and IRC discussion are corresponding to the above reaction path, which proves the reliability of the reaction mechanism.

As can be seen from Fig. 4, the O^1-H^1 bond on the catalyst in TS1 and TS4 is broken to provide Bronsted acid H to participate in the reaction, and the bond is formed in TS3 and TS6 to reduce the catalyst. The two Si-Cl bonds and two Si-O bonds in TS2 and TS5 are one broken bond and one formed bond, which indicates that the Cl groups and Si groups in the silane reactants are interchanged at this time through intermediates formed by the catalyst. Finally, in TS3 and TS6, the above Si-O bonds were broken, and at the same time, O^1, H^1 and Si, C formed bonds again respectively, so as to realize the catalyst's reduction and make Si groups return to the main product and by-products. It is suggested that the O-H bond of the catalyst can provide Bronsted acid H and transfer Si groups, making the disproportionation reaction finally possible. By analyzing the data and trends, each stage of the reaction starts from the reactant and passes through the transition state to the product. The results of IRC calculation further prove that the structure of reactants, transition states and products is reliable and the reaction mechanism is credible.

The activation energy of each reaction in Channel 1 and Channel 2 was calculated by ZPE correction, which is very important to evaluate the performance of ZSM-5(3T)@γ-Al_2O_3 core-shell catalyst. From Fig. 5 and Table 1, taking No. 1 active site as an example, the activation energy of each step of the main reaction is 107.42, 23.36 and 107.60 kJ·mol^{-1}, respectively. The activation energies of the first and third steps are obviously higher than that of the second step. If the error factor is taken into account, it indicates that the first and third steps determine the main reaction rate. Similarly, the activation energy of the last step in the side reaction channel is 139.83 kJ·mol^{-1}, which is also much higher than the activation energy of the fourth step of 105.37 kJ·mol^{-1} and the activation energy of the fifth step of 62.43 kJ·mol^{-1}. Therefore, the last step is the Rate Determining Step of the side reaction. Moreover, according to the activation energy of the main reaction and the side reaction, under the same reaction conditions, the side reaction is less likely to occur, while the main reaction is relatively easy to occur. This indicates that ZSM-5(3T)@γ-Al_2O_3 core-shell catalyst has a good catalytic effect on the disproportionation of M1 and M3 to prepare M2.

From Fig. 5 and Table 1, according to the comparison of all activation energy values of each active site, the activation energies of the RDS in main reaction are 107.60, 135.09, 134.95 and 139.38 kJ·mol^{-1}, respectively, and the activation energies of the RDS in side reaction are 139.83, 148.38, 123.92 and 129.45 kJ·mol^{-1}, respectively. The activation energies of the main reaction at reaction sites 1 and 2 are lower than those of the side reaction, that is, the main reaction is more competitive in the corresponding disproportionation reaction. The activation energies of No. 3 and No. 4 active sites for side reactions are slightly lower than those of the main reaction, that is, in the corresponding reactions, the side reactions are slightly more competitive. The probability of catalyzing the main reaction at each site is as follows: 1>2; the possibility of catalytic side reaction at each site is ranked as: 3>4. The activation energy of the main reaction at the active site No. 1 is lower than those of the side reaction at the other active sites. Therefore, ZSM-5(3T)@γ-Al_2O_3 could catalyze the main reaction successfully. This is consistent with the speculation of the reaction mechanism mentioned above. The Channel 1 generating M2 is indeed the main reaction channel, which proves the reliability of the reaction mechanism again.

The H of catalyst firstly participates in the disproportionation reaction process to generate corresponding intermediates and products, and finally returns to the catalyst through the reaction channels 1 and 2, which not only realizes the recovery of the catalyst, but also realizes the generation of main products and by-products. It is suggested that the O-H bond of the catalyst can provide Bronsted acid H and transfer Si groups, making the disproportionation reaction finally possible.

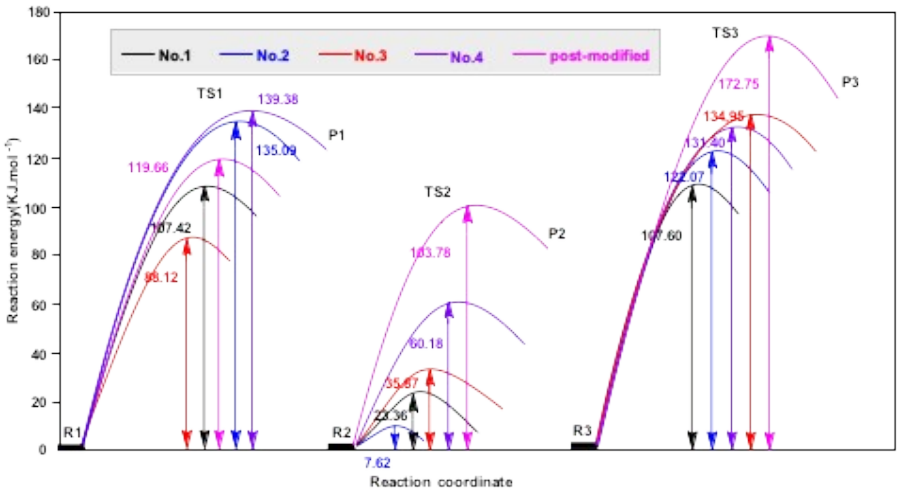

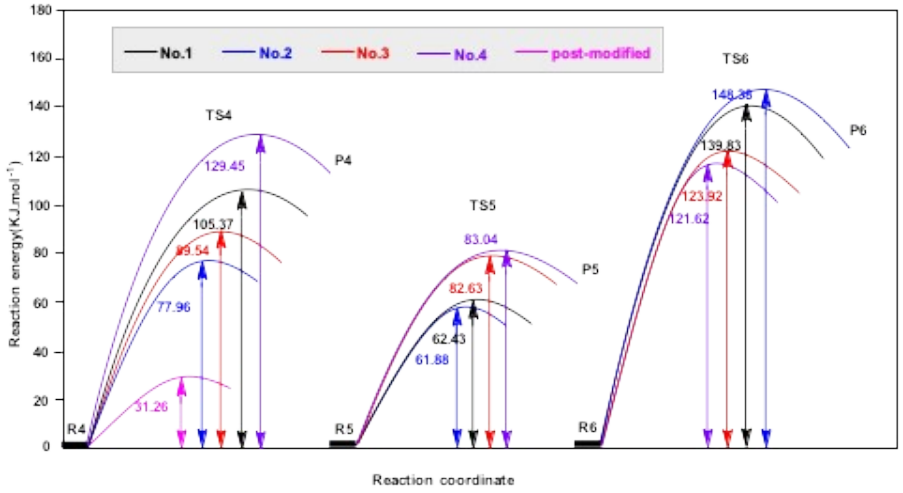

Fig. 5. Activation energies in in the catalytic system of the ZSM-5(3T)@γ-Al_2O_3 catalyst on each active site (1~4) and post-modified $AlCl_3$/ZSM-5(3T)@γ-Al_2O_3 catalyst.

Table 1 Activation energies (Ea, kJ·mol^{-1}) in the catalytic system of ZSM-5(3T)@γ-Al_2O_3 catalyst and post-modified $AlCl_3$/ZSM-5(3T)@γ-Al_2O_3 catalyst. Red and blue indicates rate-determining step activation energies of main reaction and side reaction, respectively.

		ZSM-5(3T)@γ-Al_2O_3				$AlCl_3$/ZSM-5(3T)@γ-Al_2O_3
	active site	**1**	**2**	**3**	**4**	
Activation energies(kJ.mol^{-1})	Ea_1	107.42	135.09	88.12	139.38	119.66
	Ea_2	23.36	7.62	35.87	60.18	103.78
	Ea_3	107.60	122.07	134.95	131.40	172.75
	Ea_4	105.37	77.96	89.54	129.45	31.26
	Ea_5	62.43	61.88	82.63	83.04	
	Ea_6	139.83	148.38	123.92	121.62	

3.3 $AlCl_3$/ZSM-5(3T)@γ-Al_2O_3 catalyst

In general, the reaction mechanism on the redistribution synthesis of M2 by post-modified $AlCl_3$/ZSM-5(3T)@γ-Al_2O_3 catalyst is similar to that of ZSM-5(3T)@γ-Al_2O_3 core-shell catalyst. It is clear from Fig. 6 that these reactions also occur through two channels, i.e. channel 1 and Channel 2. Rx (x=1~4) represents the reactant, Px (x=1~4) represents the product and TSx (x=1~4) represents the transition state.

In the main reaction (channel 1), the catalyst firstly reacts with $(CH_3)_3SiCl$, and the Al*-Cl* bond of the catalyst breaks and attacks the Si^1-C^1 bond in the silane, and then the product P1 (composed of intermediate I and main product $(CH_3)_2SiCl_2$) is

generated through transition state TS1; intermediate I reacts with CH_3SiCl_3 and generates P2 via TS2, which makes the catalyst be reduced and the main product $(CH_3)_2SiCl_2$ is produced. In the side reaction (channel 2), the catalyst first reacts with CH_3SiCl_3, and then passes through TS3 to P3(composed of intermediate I and by-product $SiCl_4$); finally, I reacts with $(CH_3)_3SiCl$ and generates P4 (by-product $Si(CH_3)_4$ and the catalyst reduced) through TS4. The above reaction mechanism coincided with the experimental conclusion of Jessy Lemieux et al. which further showed that the cleavage energy of Si-C bond was low and easy to fracture. It can also be seen from the figure that the active center involved in the reaction is Cl provided by Al-Cl bond, which is an obvious catalytic active center of Lewis acid.[47-49]

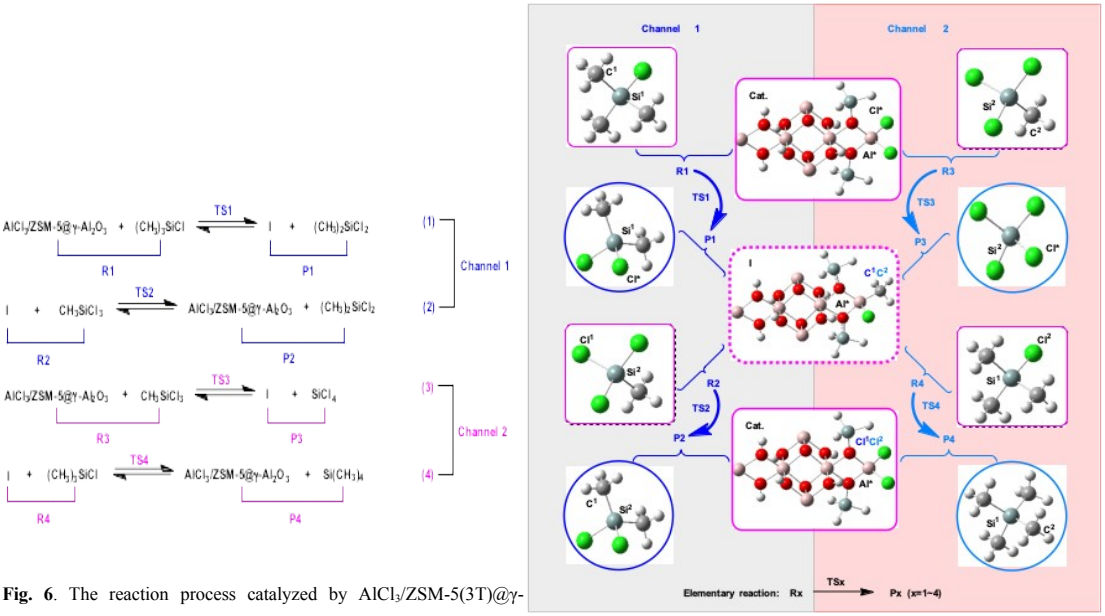

Fig. 6. The reaction process catalyzed by $AlCl_3$/ZSM-5(3T)@γ-Al_2O_3 catalyst and key atomic numbers. Rx, TSx and Px (x=1~4) represents the reactant, the transition state and the product, respectively. Cat. and I represents $AlCl_3$/ZSM-5(3T)@γ-Al_2O_3 catalyst and intermediate, respectively.

Similarly, in Fig. 6, the changes of bond length between key atoms constitute each transition state in the reaction process. In order to verify the structural accuracy of the transition state TSx (x=1~4), the virtual vibration mode diagrams of the transition states were obtained by using vibration analysis and calculation, as shown in Fig. 7 and Fig. S5. In addition, shown in Fig. 8, IRC method was used to track the Forward and Reverse directions of transition states and the reliability of transition states was determined. Wherein negative, positive and zero represent reactants, products and transition states, respectively. Combined with Fig. 6, Fig.7, Fig. S5 and Fig. 8, in channel 1, the atomic spacing of Al*-Cl* changes from 0.2205 nm to 0.5022 nm, and the atomic spacing of C^1-Si^1 changes from 0.1899 nm to 0.4244 nm, indicating that Al*-Cl* and C^1-Si^1 bonds gradually separated and finally broken. At the same time, the spacing between Cl* and Si^1 changes 0.4090 nm to 0.2182 nm, and the spacing between Al* and C^1 changes from 0.4855 nm to 0.1966 nm. Finally, Cl*-Si^1 and Al*-C^1 bonds are formed. At this time, the transition state TS1 moves towards its corresponding product P1. Then atoms in Si^2-Cl^1 and Al*-C^1 bonds gradually move away and finally bonds break, Si^2, C^1 and Al*, Cl^1 move close to each other and finally form bonds. Compared with the initial atomic distance of C^1-Si^2 (0.5415 nm) and Cl^1-Al* (0.3932 nm) of the reactant (R2), the distance significantly decreases to 0.1886 nm and 0.2212 nm in the product P2, respectively. At this time, the transition state TS2 moves towards its product P2. Observing another

vibrational direction of the key atoms in TS1, C^1 atom gradually approach and bond with Si^1 atom. Al* atom and Cl* atom move closely to each other and bond finally to form its corresponding reactant R1. Other transition states can be analyzed in a similar way. The transition states in channel 2 can also move to their respective reactants and products through the corresponding atomic vibration. The longitudinal or radial stretching vibration between the key atoms is equivalent, which proves that the calculated transition state structure is correct. It can also be seen from Fig. 7 and Fig. S5 that the catalytic active center is the Cl* of Lewis acid center. The Cl* firstly participates in the disproportionation reaction process to generate intermediate and products, and finally returns to the catalyst through the reaction channels 1 and 2, which not only realizes the recovery of the catalyst, but also realizes the generation of main products and by-products. The vibration analysis and IRC discussion are corresponding to the above reaction path, which proves the reliability of the reaction mechanism.

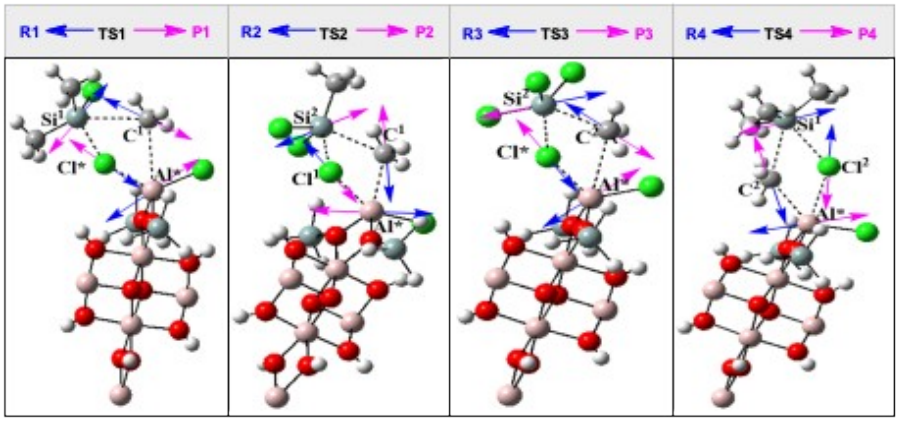

Fig. 7. The virtual vibration modes of transition states in the reaction process of post-modified $AlCl_3$/ZSM-5(3T)@γ-Al_2O_3 catalyst.

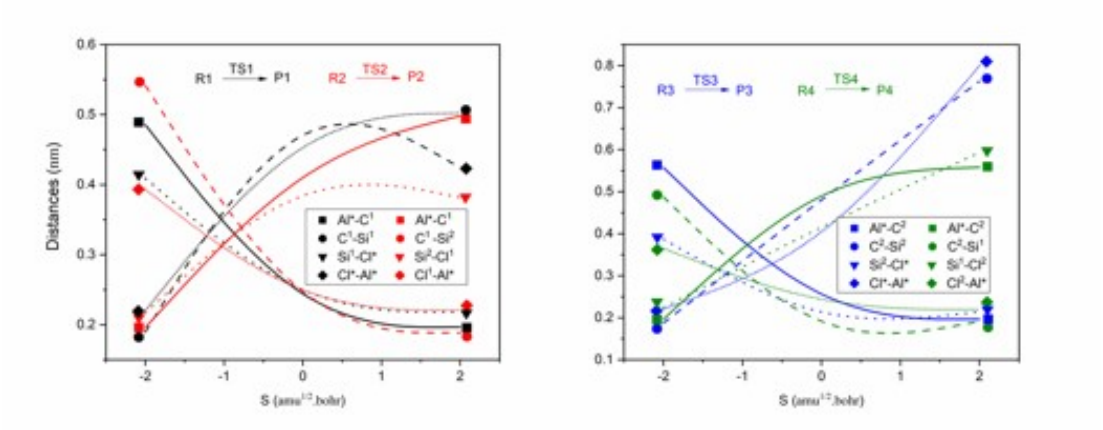

Fig. 8. The spacing trends of key atoms along IRC in the catalytic system of the $AlCl_3$/ZSM-5(3T)@γ-Al_2O_3 catalyst.

The activation energy of each reaction in Channel 1 and Channel 2 was calculated by ZPE correction, which plays a critical role in evaluating the performance of $AlCl_3$/ZSM-5(3T)@γ-Al_2O_3 core-shell catalyst. From Fig. 5 and Table 1, the activation energy of each step of the main reaction is 119.66 and 103.78 kJ·mol^{-1}, respectively. The activation energy of the first step is

obviously higher than that of the second step. If the error factor is taken into account, it indicates that the first step determines the main reaction rate. Similarly, the activation energy of the third step in the side reaction channel is 172.75 kJ·mol^{-1}, which is also much higher than the activation energy of the fourth step of 31.26 kJ·mol^{-1}. Therefore, the last step is the Rate Determining Step of the side reaction. Moreover, according to the activation energy of the main reaction and the side reaction, under the same reaction conditions, the side reaction is less likely to occur, while the main reaction is relatively easy to occur. This indicates that $AlCl_3$/ZSM-5(3T)@γ-Al_2O_3 core-shell catalyst has a good catalytic effect on the disproportionation of M1 and M3 to prepare M2.

From Table 1, according to the activation energy values of No.1 and No.2 active sites in the ZSM-5(3T)@γ-Al_2O_3 core-shell catalyst system and that of $AlCl_3$/ZSM-5(3T)@γ-Al_2O_3 core-shell catalyst system, the activation energies of the RDS in main reaction are 107.60, 135.09 and 119.66 kJ·mol^{-1}, respectively, and the activation energies of the RDS in side reaction are 139.83, 148.38 and 172.75 kJ·mol^{-1}, respectively. The activation energies difference between main reaction and side reaction in the $AlCl_3$/ZSM-5(3T)@γ-Al_2O_3 core-shell catalyst system are higher than those of ZSM-5(3T)@γ-Al_2O_3 core-shell catalyst system, that is, the side reaction is less competitive in the corresponding disproportionation reaction. Therefore, $AlCl_3$/ZSM-5(3T)@γ-Al_2O_3 could be in favor of catalyzing the main reaction comparing with ZSM-5(3T)@γ-Al_2O_3. This is consistent with the speculation of the reaction mechanism mentioned above. The channel 1 generating M2 is indeed the main reaction channel, which proves the reliability of the reaction mechanism again.

From Table 2, the bond order analysis of two Al*-Cl* bonds were performed. The bond order of Al*-Cl*^{2} including single bond's Mayer bond order (MBO), Laplacian bond order (LBO) and Mulliken bond order is higher than that of Al*-Cl*^{1}, indicating that Al*-Cl*^{1} is easy to broke and the reaction is more likely to occur. Besides, the Multi-centers bond order of Al*-Cl*^{1}-O^1-O^2 is higher than that of Al*-Cl*^{2}-O^1-O^2, indicating that the Al*-Cl*^{1}-O^1-O^2 bond of post-modified catalyst has better stability, that is, the loaded location of Al*-Cl*^{1} is more stable than the other one. It is suggested that only one Cl atom can participate in the reaction process, ascribing to the sterichindrance effect and the channel confinement effect. This is consistent with the speculation of the reaction mechanism mentioned above. The catalytic active site Cl*^{1} is indeed in favor of participating in the reaction, which proves the reliability of the reaction mechanism again.

Table 2 The bond order of different active sites in the post-modified $AlCl_3$/ZSM-5 (3T)@γ-Al_2O_3 catalyst system.

Al-Cl bond order	MBO	LBO	Mulliken	Al-Cl-O^1-O^2 bond order
Al*-Cl*^{1}	0.8201	0.1965	0.3980	0.0015
Al*-Cl*^{2}	0.8205	0.1966	0.3985	0.0014

According to our previous works, the most optimization activation energies of the RDS in main reaction and side reaction in the catalytic system of $AlCl_3$/ZSM-5(3T) are 111.60 and 155.60 kJ·mol^{-1}, while those are 107.60 and 139.83 kJ·mol^{-1} in the catalytic system of ZSM-5(3T)@γ-Al_2O_3 and 119.66 and 172.75 kJ·mol^{-1} in the catalytic system of $AlCl_3$/ZSM-5(3T)@γ-Al_2O_3, respectively.[22] That is to say that the activation energy of main reaction rate determining step of $AlCl_3$/ZSM-5(3T) catalyst is nearly similar to that of ZSM-5(3T)@γ-Al_2O_3 and $AlCl_3$/ZSM-5(3T)@γ-Al_2O_3. However, the difference value of activation energy between rate determining steps in the main reaction and the side reaction of $AlCl_3$/ZSM-5(3T)@γ-Al_2O_3 catalyst is the

highest, which illustrate that the side reaction is prohibited much more and the main reaction is permitted as well. So, $AlCl_3$/ZSM-5(3T)@γ-Al_2O_3 has the best catalytic reactivity.

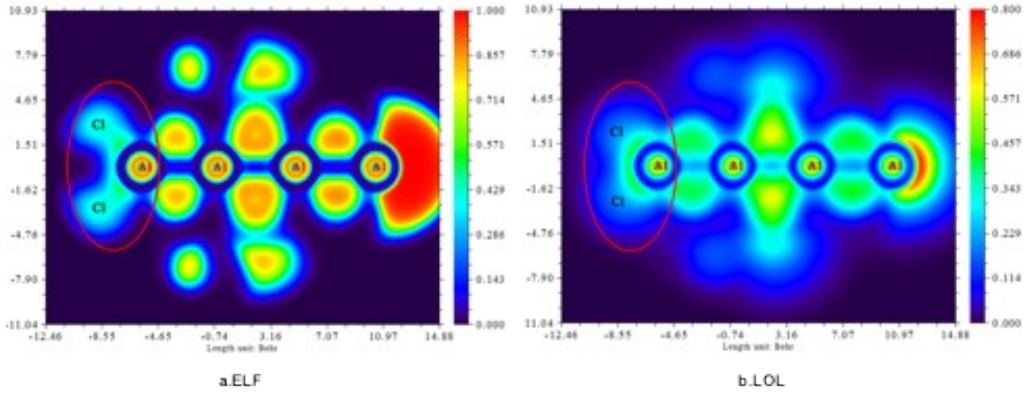

Fig. 9. (a) ELF and LOL (b) analysis of the post-modified $AlCl_3$/ZSM-5(3T)@γ-Al_2O_3 catalyst.

On the other hand, the Electronic Localization Function (ELF) and the Localized Orbit Locator (LOL) analysis were carried out to explain catalytic character in Fig. 9. Wherein dark blue and red indicates robust electronic delocalization and little electronic delocalization. From Fig. 9 (a), in the interior of Al atom and Cl atom, bright color like orange and green indicates robust electronic localization. Oppositely, blue-violet outside of Al atom and Cl atom shows robust electronic delocalization, and therefore facilitates the shared electron between Al atom and Cl atom. Similarly, it is obvious that bright color like yellow and green (represents robust electronic localization) gradually transfers to blue (represents robust electronic delocalization) from the center to the margin of both Al atom and Cl atom. Obviously, the difference between interior and external both Al atom and Cl atom can be good agreement with the result of ELF as it shown in Fig. 9 (b). In conclusion, electronic delocalization of Cl atom and strong electronic localization of Al atom facilitates electrons move close to Si atom and the electronic attracking from methyl group in silane, respectively. Therefore, ELF and LOL confirm that Lewis acid of the catalyst modified with $AlCl_3$ is strengthened and the credible of redistribution reaction, which demonstrates that the active site as the Lewis acidic center is in agreement with the previous studies, plays a critical role in the explanation of the nature of the reaction.

4 Conclusions

In this paper, the redistribution synthesis mechanism of M2 over ZSM-5(3T)@γ-Al_2O_3 core-shell catalyst and post-synthesis $AlCl_3$/ZSM-5(3T)@γ-Al_2O_3 catalyst has been investigated by using the DFT method. (1) Among the ZSM-5(3T)@γ-Al_2O_3 core-shell catalyst, H atom of Bronsted acid is active site and the No.1 active site has the best catalytic performance. (2) The $AlCl_3$/ZSM-5(3T)@γ-Al_2O_3 core-shell catalyst has Lewis acid active site Al-Cl bond, which has a better catalytic effect than ZSM-5(3T)@γ-Al_2O_3. (3) The structures of catalytic systems, the virtual vibration models of the transition states IRC, the spacing trends of key atoms along IRC, energy calculations, the parameters of various kinds of bond orders, ELE and LOL analysis completely are consistent with each other.

Acknowledgements

The authors gratefully acknowledge the support of the National Natural Science Foundation of China (No. 21563011 and 21872049). Thanks very much for Professor Sanguo Hong's help.

Conflict of interest

The authors declare that they have no known competing financial interests or personal relationships that could have appeared to influence the work reported in this paper.

References

[1] R. Savela, H. Grénman, H. Sundelin, P.-O. Norrby, D. Yu. Murzin, R. Leino, Kinetic and Theoretical Investigation of Iron(III)-Catalyzed Silane Chlorination.ChemCatChem. 8 (2016) 584-592.

[2] H. Chen, M. Yang, W. Shang, Y. Tong, B. Liu, X. Han, J. Zhang, Q. Hao, M. Sun, X. Ma, Organosilane Surfactant-Directed Synthesis of Hierarchical ZSM-5 Zeolites with Improved Catalytic Performance in Methanol-to-Propylene Reaction.Industrial & Engineering Chemistry Research. 57 (2018) 10956-10966.

[3] X. Li, P. Zhang, G. Chen, W. Wang, J. Li, Waste minimization and efficient disposal of particles in optimized organic silicon production.Journal of Cleaner Production. 242 (2020).

[4] H. L. Castricum, A. Sah, M. C. Mittelmeijer-Hazeleger, J. E. ten Elshof, Hydrophobisation of mesoporous γ-Al_2O_3 with organochlorosilanes—efficiency and structure.Microporous and Mesoporous Materials. 83 (2005) 1-9.

[5] Y. Tian, W. Zhang, M. Ge, S. Yu, X. Lv, T. Zhang, Polymerization of methylsilylenes into polymethylsilanes or polycarbosilanes after dechlorination of dichloromethylsilanes?RSC Advances. 6 (2016) 21048-21055.

[6] P. A. Gushchin, I. M. Kolesnikov, V. A. Vinokurov, E. V. Ivanov, V. A. Lyubimenko, V. N. Borshch, Alkylation of benzene with ethylene in the presence of dimethyldichlorosilane.Journal of Catalysis. 352 (2017) 75-82.

[7] M. Okamoto, S. Onodera, Y. Yamamoto, E. Suzuki, Y. Ono, Direct synthesis of organodichlorosilanes by the reaction of metallic silicon, hydrogen chloride and alkene/alkyne and by the reaction of metallic silicon and alkyl chloride.Journal of the Chemical Society, Dalton Transactions. (2001) 71-78.

[8] J. Li, Z. Ni, Y. Ji, Y. Zhu, H. Liu, Y. Zhang, X.-Q. Gong, Z. Zhong, F. Su, ZnO supported on Cu_2O{1 0 0} enhances charge transfer in dimethyldichlorosilane synthesis.Journal of Catalysis. 374 (2019) 284-296.

[9] K. Janmanchi, A. Coppernoll, D. Katsoulis, Two-Step Process for the Synthesis of Dimethyldichlorosilane Using Copper Aluminate Catalysts.Industrial & Engineering Chemistry Research. 59 (2020) 3321-3333.

[10] H. Watson, A. E. E. Norström, J. G. Matisons, A. Root, J. B. Rosenholm, Deposition of amine functional silanes onto E-glass fibres, an NMR study.Journal of Adhesion Science and Technology. 15 (2001) 1103-1117.

[11] K. Arnby, M. Rahmani, M. Sanati, N. Cruise, A. A. Carlsson, M. Skoglundh, Characterization of Pt/γ-Al_2O_3 catalysts deactivated by hexamethyldisiloxane.Applied Catalysis B: Environmental. 54 (2004) 1-7.

[12] Q. Fu, N. Zhang, J. Zhang, S. Hong, Catalytic Disproportionation of Methyltrichlorosilane by AL-MCM-41 to Prepare Dichlorodimethylsilane.Phosphorus, Sulfur, and Silicon and the Related Elements. 187 (2012) 1183-1194.

[13] Y. Jiang, W. Chen, Y. Liu, H. Yin, Y. Shen, A. Wang, L. Yu, T. Jiang, Synthesis of Trimethylchlorosilane by [BMIM]Cl−n$AlCl_3$ Ionic Liquids-Catalyzed Redistribution between Methyltrichlorosilane and Low-Boiling Products from the Direct Synthesis of Methylchlorosilanes.Industrial & Engineering Chemistry Research. 50 (2011) 1893-1898.

[14] W. A. Harding, S. Harold, Disproportionation of siliconhalides, in, US, 1967.

[15] W. Xu, M. Yang, X. Li, S. Yang, X. Chen, Z. Fang, X. Wu, S. Hong, CALCULATION OF CATALYTIC REACTIVITY FOR PREPARING DICHLORODIMETHYLSILANE UTILIZING PRE- AND POST-MODIFIED 24T $AlCl_3$/ZSM-5.Química Nova. (2017).

[16] M. Nieminen, L. Niinist, Determination of aluminium in $AlCl_3$ and Al_2O_3 modified silica catalyst supports.Fresenius' Journal of Analytical Chemistry. 364 (1999) 224-227.

[17] A. L. Petre, W. F. Hoelderich, M. L. Gorbaty, Dodecylbenzene transformations: Dealkylation and disproportionation over immobilized ionic liquid catalysts.Applied Catalysis A: General. 363 (2009) 100-108.

[18] Y.-H. Lai, L. S. Benner, K. P. C. Vollhardt, Studies on the reaction of benzene and other hydrocarbons with aluminium trichloride: Effect of catalytically activated hydrogen.Fuel. 63 (1984) 231-238.

[19] Z.-K. Chu, G. Fu, X. Xu, Theoretical studies of Na+ location in ZSM-5: Model selection for accurate coordination structure and energetics.Catalysis Today. 165 (2011) 112-119.

[20] X. Wenyuan, M. Yang, X. Li, S. Yang, X. Chen, Z. Fang, X. Wu, S. Hong, Study on the Mechanism of Methylchlorosilanes Disproportionation Catalyzed by $AlCl_3/(AlCl_2)_Z^{Z+}$-γ-Al_2O_3[1].Russian Journal of Physical Chemistry A. 92 (2019) 2634-2639.

[21] W. Xu, F. Yan, S. Yang, Z. Guo, L. Hu, Z. He, S. Hong, Mechanism on The Disproportionating Synthesis of Dichlorodimethyl- silane by ZSM-5(5 T)@γ-Al_2O_3 SeriesCore-Shell Catalysts.Applied Organometallic Chemistry. 34 (2019).

[22] W. Xu, M. Yang, Y. Liu, Z. Guo, L. Hu, S. Yang, S. Hong, Disproportionation mechanism of methylchlorosilanes catalyzed by different clusters $AlCl_3$/ZSM-5.Journal of Chemical Sciences. 130 (2018).

[23] W. Xu, Y. Wang, S. Li, Y. Cheng, F. Yan, L. Hu, M. Liao, J. Peng, Z. Guo, ZSM-5(8T)@gamma-Al2O3 supported AlCl3 core-shell catalyst: Mechanism research on disproportionation reaction of methylchlorosilanes.Inorganica Chimica Acta. 516 (2021).

[24] W. Xu, Y. Wang, S. Li, Y. Cheng, Z. Guo, L. Hu, M. Liao, J. Peng, X. Chen, S. Yang, Study on the mechanism of catalytic synthesis of dimethyldichlorosilane by $AlCl_3$/MIL−53(Al)@γ−Al_2O_3.Applied Organometallic Chemistry. 35 (2020).

[25] V. N. Solkan, G. M. Zhidomirov, Post-Hartree-Fock (MP2 and MP4) study on decomposition of nitrous oxide on the nonframework AlO(+) site in ZSM-5 zeolite.International Journal of Quantum Chemistry. 111 (2011) 2639-2648.

[26] V. N. Solkan, G. M. Zhidomirov, MP2 study on decomposition of nitrous oxide on the Ga-ZSM-5.International Journal of Quantum Chemistry. 108 (2008) 2732-2743.

[27] A. Abdalla, P. Arudra, S. S. Al-Khattaf, Catalytic cracking of 1-butene to propylene using modified H-ZSM-5 catalyst: A comparative study of surface modification and core-shell synthesis.Applied Catalysis A: General. 533 (2017) 109-120.

[28] S. Jiang, Y. Du, M. Marcello, E. W. Corcoran, Jr., D. C. Calabro, S. Y. Chong, L. Chen, R. Clowes, T. Hasell, A. I. Cooper, Core-Shell Crystals of Porous Organic Cages.Angew Chem Int Ed Engl. 57 (2018) 11228-11232.

[29] R. Lu, M. Xu, B. Fu, Y. Zhang, C. Zhou, Y. Zeng, S. Yang, X. Song, X. Zhou, Single Capillary Electrospinning of Magnetic Core-shell Nanofibers.ChemistrySelect. 1 (2016) 1510-1514.

[30] P. Wang, H. Tooriyama, K. Yokoyama, M. Ohtani, H. Asahara, T. Konishi, N. Nishiwaki, M. Shimoda, Y. Yamashita, H. Yoshikawa, K. Kobiro, Smart Decoration of Mesoporous TiO_2 Nanospheres with Noble Metal Alloy Nanoparticles into Core-Shell, Yolk-Core-Shell, and Surface-Dispersion Morphologies.European Journal of Inorganic Chemistry. 2014 (2014) 4254-4257.

[31] R. S. Ghosh, T. T. Le, T. Terlier, J. D. Rimer, M. P. Harold, D. Wang, Enhanced Selective Oxidation of Ammonia in a Pt/Al_2O_3@Cu/ZSM-5 Core–Shell Catalyst.ACS Catalysis. 10 (2020) 3604-3617.

[32] S. Ryu, H. W. Lee, Y.-M. Kim, J. Jae, S.-C. Jung, J.-M. Ha, Y.-K. Park, Catalytic fast co-pyrolysis of organosolv lignin and polypropylene over in-situ red mud and ex-situ HZSM-5 in two-step catalytic micro reactor.Applied Surface Science. 511 (2020).

[33] Z. Li, W. Wang, X. Wang, Z. Quan, Mechanism of Synthesis of Phosphinecarboxamides by Reaction of Sodium Phosphaethynolate Anion and Amines under Acid-Free Conditions: Density Functional Theory Investigation.Chinese Journal of Organic Chemistry. 40 (2020).

[34] M. U. Khan, M. Y. Mehboob, R. Hussain, R. Fatima, M. S. Tahir, M. Khalid, A. A. C. Braga, Molecular designing of high−performance 3D star−shaped electron acceptors containing a truxene core for nonfullerene organic solar cells.Journal of Physical Organic Chemistry. (2020).

[35] M. H. Mahyuddin, A. Staykov, A. G. Saputro, M. K. Agusta, H. K. Dipojono, K. Yoshizawa, Novel Mechanistic Insights into Methane Activation over Fe and Cu Active Sites in Zeolites: A Comparative DFT Study Using Meta-GGA Functionals.The Journal of Physical Chemistry C. 124 (2020) 18112-18125.

[36] M. Abdelgaid, J. Dean, G. Mpourmpakis, Improving alkane dehydrogenation activity on γ-Al2O3 through Ga doping.Catalysis Science & Technology. 10 (2020) 7194-7202.

[37] Z. P. Deng, D. G. Zhou, Mechanisms of Csp^3−H or Nsp^2−H functionalization of 2,3−diaminoindoles with triplet O_2: A density functional theory investigation.Journal of Physical Organic Chemistry. (2020).

[38] N. Zhang, C. Liu, J. Ma, R. Li, H. Jiao, Determining the structures, acidity and adsorption properties of Al substituted HZSM-5.Phys Chem Chem Phys. 21 (2019) 18758-18768.

[39] P. Hirunsit, K. Faungnawakij, S. Namuangruk, C. Luadthong, Catalytic behavior and surface species investigation over γ-Al_2O_3 in dimethyl ether hydrolysis.Applied Catalysis A: General. 460-461 (2013) 99-105.

[40] J. Sun, W.-C. Lu, W. Zhang, L.-Z. Zhao, Z.-S. Li, C.-C. Sun, Theoretical study on $(Al_2O_3)_n$ (n = 1-10 and 30) fullerenes and H_2 adsorption properties.ChemInform. 39 (2008) 2274-2279.

[41] Z. Wen, S. Li, H. Li, Y. Li, G. Wang, Quantum Chemical Study on the Reaction Mechanism of Fast SCR Catalyzed by ZSM-5 Doped with Mn/Co–Al/Ce.Arabian Journal for Science and Engineering. 44 (2019) 5549-5557.

[42] M. Trombetta, T. Armaroli, A. d. Gutièrrez Alejandre, J. Ramirez Solis, G. Busca, An FT-IR study of the internal and external surfaces of HZSM5 zeolite.Applied Catalysis A: General. 192 (2000) 125-136.

[43] K. Chen, M. Abdolrahmani, S. Horstmeier, T. N. Pham, V. T. Nguyen, M. Zeets, B. Wang, S. Crossley, J. L. White, Brønsted–Brønsted Synergies between Framework and Noncrystalline Protons in Zeolite H-ZSM-5.ACS Catalysis. 9 (2019) 6124-6136.

[44] W. Dai, C. Wang, X. Yi, A. Zheng, L. Li, G. Wu, N. Guan, Z. Xie, M. Dyballa, M. Hunger, Identification of tert-Butyl Cations in Zeolite H-ZSM-5: Evidence from NMR Spectroscopy and DFT Calculations.Angew Chem Int Ed Engl. 54 (2015) 8783-8786.

[45] D. S. A. Silva, W. N. Castelblanco, D. H. Piva, V. de Macedo, K. T. G. Carvalho, E. A. Urquieta-González, Tuning the Brønsted and Lewis acid nature in HZSM-5 zeolites by the generation of intracrystalline mesoporosity—Catalytic behavior for the acylation of anisole.Molecular Catalysis. 492 (2020).

[46] Z. Yan, Z. Zuo, Z. Li, J. Zhang, A cluster DFT study of NH_3 and NO adsorption on the $(MoO_2)^{2+}$/HZSM-5 surface: Lewis versus Brønsted acid sites.Applied Surface Science. 321 (2014) 339-347.

[47] J. Yang, L. Chang, L. Jiang, K. Wang, L. Huang, Z. He, H. Shao, J. Wang, C.-n. Cao, Electrodeposition of Al-Mn-Zr ternary alloy films from the Lewis acidic aluminum chloride-1-ethyl-3-methylimidazolium chloride ionic liquid and their corrosion properties.Surface and Coatings Technology. 321 (2017) 45-51.

[48] T. Krahl, E. Kemnitz, The very strong solid Lewis acids aluminium chlorofluoride (ACF) and bromofluoride (ABF)—Synthesis, structure, and Lewis acidity.Journal of Fluorine Chemistry. 127 (2006) 663-678.

[49] S. Kiatphuengporn, A. Junkaew, C. Luadthong, S. Thongratkaew, C. Yimsukanan, S. Songtawee, T. Butburee, P. Khemthong, S. Namuangruk, M. Kunaseth, K. Faungnawakij, Roles of acidic sites in alumina catalysts for efficient d-xylose conversion to lactic acid.Green Chemistry. (2020).

Supporting information

Additional supporting information may be found online in the Supporting Information section.